



# Photoelectrocatalytic regeneration of NADH at poly(4,4'-diaminodiphenyl sulfone)/nano TiO<sub>2</sub> composite film modified indium tin oxide electrode

Ya-Hui Ho, Arun Prakash Periasamy, Shen-Ming Chen\*

Department of Chemical Engineering and Biotechnology, National Taipei University of Technology, No. 1, Section 3, Chung-Hsiao East Road, Taipei 106, Taiwan, ROC

## ARTICLE INFO

### Article history:

Received 25 November 2010

Received in revised form 12 March 2011

Accepted 30 March 2011

Available online 7 April 2011

### Keywords:

Poly(4,4'-diaminodiphenyl sulfone)

TiO<sub>2</sub> nanoparticles

NADH

Photoregeneration

Photoelectrocatalysis

## ABSTRACT

Herein we report the photoelectrocatalytic regeneration of NADH at poly(4,4'-diaminodiphenyl sulfone)/nano TiO<sub>2</sub> (PDDS/TiO<sub>2</sub>) composite modified indium tin oxide (ITO) electrode. The PDDS film growth was confirmed through in situ electrochemical quartz crystal microbalance (EQCM) studies. The prepared PDDS/TiO<sub>2</sub> composite was characterized by scanning electron microscopy (SEM), atomic force microscopy (AFM) and X-ray diffraction (XRD) studies. SEM and AFM results confirmed that TiO<sub>2</sub> nanoparticles size is between 130 and 180 nm. XRD results showed that TiO<sub>2</sub> nanoparticles are crystalline and belong to anatase phase. Electrochemical impedance spectroscopy (EIS) and light induced EIS results substantiate a rapid electron transfer process at PDDS/TiO<sub>2</sub> composite surface. Cyclic voltammetry (CV) results demonstrated that composite film showed excellent response to the photoelectrocatalytic regeneration of NADH. The photoelectrocatalytic oxidation of NADH at composite film surface irradiated for 5 min (optimized irradiation time) produced a notable enhancement in anodic peak current and it was 18-fold higher than that of PDDS film and several folds higher than that of TiO<sub>2</sub> and bare ITO electrodes. Further, composite film showed higher sensitivity of 124.1  $\mu\text{A } \mu\text{M}^{-1}$  for NADH. From Square wave voltammetry (SWV) results, sensitivity of the irradiated composite film was obtained as 0.252  $\mu\text{A nM}^{-1}$  of NADH. The linear concentration range was between 23 and 39 nM NADH respectively. Further, the composite film exhibits good selectivity towards NADH and no significant interference effect was observed even when 200-fold excess of ascorbic acid (AA), dopamine (DA) and uric acid (UA) coexist in the same supporting electrolyte solution.

© 2011 Elsevier B.V. All rights reserved.

## 1. Introduction

The redox electrochemistry and meticulous interconversion pathway of nicotinamide adenine dinucleotide (NAD<sup>+</sup>) and its reduced form (NADH) have fascinated immense interest since they play critical role as redox coenzymes in biological systems [1]. Significant advancements have been made in this area of research promptly after the exploitation of chemically modified electrodes [2]. However, an important shortcoming was direct oxidation of NADH at conventional solid electrode surfaces often required high over potential [3,4]. As a result significant interference effect would be caused by easily oxidizable species [5]. Furthermore, these oxidizable products and the radical intermediates formed during NADH oxidation reaction pathway would pacify the electrode surfaces [6,7]. The above said shortcomings have ultimately necessitated the quest for novel electroactive materials with appreciable catalytic properties. Among various electroactive materials, redox mediators significantly reduced the over potential for NADH ox-

idation [6]. Phenoxazine [8], phenothiazines and phenazines groups containing mediators were used in larger extent in NADH sensors [9–13]. However, rapid deactivation of mediators on electrode surface causes electrode surface poisoning and blocking [14,15].

In recent years, with progressive advancements in the field of nanotechnology, considerable interest has been drawn towards the exploitation of nanomaterials in NADH based electrochemical sensors. In particular, the unique properties of CNT such as large active surface area, high electronic conductivity, high mechanical resistance properties, anti-fouling capability [16] and their ability to reduce over potential for NADH [17–21] have promoted their extensive applications in NADH based sensors [22]. Besides CNT, Au nanoparticles [5,23–25] and several conducting polymer matrices [26–34] have also been successfully employed.

Other convincing matrices used for NADH sensing applications were semiconductor nanoparticles which are well known for their unique photophysical, electronic features and enhanced electron–hole transfer efficiency [35,36]. Amid various semiconductor nanoparticles, owing to the large surface area, large band gap energy (3.2 eV) and rapid electron–hole pair generation ability, TiO<sub>2</sub> nanoparticles were extensively employed in photoelectrochemical cell and solar cell applications [37]. Particularly, studies

\* Corresponding author. Tel.: +886 2270 17147; fax: +886 2270 25238.  
E-mail address: [smchen78@ms15.hinet.net](mailto:smchen78@ms15.hinet.net) (S.-M. Chen).

related to the photocatalytic regeneration and photocatalytic oxidation of NADH at TiO<sub>2</sub> nanoparticles modified matrices have attracted much attention. Earlier, Jiang et al. studied the photocatalytic regeneration of NADH at carbon-containing TiO<sub>2</sub> in the presence of visible light and Rhodium complex catalyst [38]. In another approach, Chen et al. have noticed a good enhancement in the photocatalytic NADH regeneration at TiO<sub>2</sub> nanoparticles doped Boron upon UV light irradiation [39]. So far, the photoelectrocatalytic oxidation of NADH was successfully investigated at electropolymerized toluidine blue O and polyphenothiazine formaldehyde modified matrices [40,41]. Recently, Wang et al. have reported the photoelectrocatalytic NADH oxidation at dopamine sensitized nanoporous TiO<sub>2</sub> film and they confirmed that generated anodic photocurrent results from the absorption of visible light by dopamine–Ti charge transfer complex [42].

On the other hand, 4,4'-diaminodiphenyl sulfone (DDS) was a well known curing agent for epoxy resins [43]. Manishankar et al. reported the electrochemical preparation of conducting copolymers of DDS and aniline and investigated their electrochromic behavior through spectroelectrochemical analysis [44]. They also pioneered the chemical [45] and electrochemical [46] synthesis of copolymers containing DDS. However, to the best of our knowledge no one has reported the photoelectrocatalytic regeneration of NADH at poly(4,4'-diaminodiphenyl sulfone)/nano TiO<sub>2</sub> (PDDS/TiO<sub>2</sub>) composite. The composite film showed excellent photoelectrocatalytic response towards NADH oxidation with good sensitivity. Further, the photoelectrocatalytic current noticed at composite film increased linearly with increase in irradiation time and sequential NADH concentration additions. The photoelectrocatalytic results achieved in the present study could thus be an initiative for the construction of dehydrogenase enzyme based biosensors and other energy storage devices based on PDDS/TiO<sub>2</sub> nanocomposites.

## 2. Experimental

### 2.1. Reagents and apparatus

DDS and β-nicotinamide adenine dinucleotide, reduced sodium salt hydrate (NADH) were purchased from Sigma–Aldrich and used as received. Nano TiO<sub>2</sub> suspension was purchased from Ever light chemicals, Taiwan and used without any purification. All reagents used in this work were of analytical grade and all aqueous solutions were prepared using doubly distilled water. Prior to each experiment, experimental solutions were deoxygenated with pre-purified N<sub>2</sub> gas for 10 min and N<sub>2</sub> atmosphere was maintained above the solutions.

Cyclic voltammetry (CV) experiments were carried out using CHI 1205a work station. Similarly, Square wave voltammetry (SWV) studies were performed using CHI 750 work station. A conventional three electrode cell with 0.1 M H<sub>2</sub>SO<sub>4</sub> as supporting electrolyte was used throughout the electrochemical studies. For electrochemical experiments, ITO electrode coated either with nano TiO<sub>2</sub> or PDDS or PDDS/TiO<sub>2</sub> films was used as working electrode and Pt wire with 0.5 mm diameter was used as counter electrode. All the potentials were referred with respect to standard Ag/AgCl reference electrode. For electrochemical quartz crystal microbalance (EQCM) studies an 8 MHz AT-cut quartz crystal coated with Au was used as working electrode. The diameter of quartz crystal and Au electrode used were about 13.7 and 5 mm respectively. EIM6ex ZAHNER (Kroach, Germany) was used for electrochemical impedance spectroscopy (EIS) and ZAHNER controlled intensity modulated photo spectroscopy (CIMPS) system was used for light induced EIS and photoelectrocatalytic studies. A light emitting diode (WLL01) with an average intensity of 4u (W/m<sup>2</sup>) was used as white light source. A normalized intensity/Volt

of 1 (WV<sup>-1</sup> m<sup>-2</sup>) 472, 25 (nm, Δnm) was employed throughout the photoelectrocatalytic experiments. Where, nm is the dominant wave length and Δnm is the bandwidth of the illuminator. Surface morphology of the prepared films were studied using Hitachi S-3000 H scanning electron microscope (SEM) and Being nano-instruments CSPM 4000, atomic force microscope (AFM). UV–vis absorption spectroscopy measurements were carried out using Hitachi U-3300 spectrophotometer.

### 2.2. Preparation of PDDS/TiO<sub>2</sub> composite film modified ITO electrode

Prior to modification, ITO electrodes were cleaned well, sonicated in acetone–water mixture for 15 min and were dried at room temperature. A clean ITO electrode surface was immersed into 4 ml of TiO<sub>2</sub> nanoparticles/ethanol suspension and kept undisturbed for 20 min. The prepared nano TiO<sub>2</sub> modified ITO was taken out carefully and gently washed few times with doubly distilled water to remove loosely adsorbed TiO<sub>2</sub> nanoparticles. Finally it was dried in air for few minutes and transferred to an electrochemical cell with 0.5 mM DDS in 0.1 M H<sub>2</sub>SO<sub>4</sub>. The electropolymerization of PDDS film on nano TiO<sub>2</sub>/ITO was carried out according to the procedure reported elsewhere in literature [44]. 20 consecutive CV potential cycling were done in the potential range between –0.25 and 1.25 V at the scan rate of 100 mV s<sup>-1</sup> (figure not shown). In the first cycle a broad oxidation peak with enhanced anodic peak current appeared at 1.165 V. However, this anodic peak current decreased drastically in the consecutive cycles. As reported previously by Manishankar et al. this oxidation peak was attributed to the oxidation of amino group in the phenyl ring of DDS [44]. Finally, the prepared PDDS/TiO<sub>2</sub> modified ITO was washed gently with double distilled water and utilized for the electrochemical studies.

The isoelectric point of TiO<sub>2</sub> is 6.5, so the surface charge of TiO<sub>2</sub> is negative at pH above the isoelectric point and positive at pH below the isoelectric point [47]. It is noteworthy that, pH of the TiO<sub>2</sub> suspension used in this study is 6.3 and since this value lies below the isoelectric point, the surface charge of TiO<sub>2</sub> NPs is positive. Whereas, the PDDS used in this study is an anionic polymer and therefore its surface is negatively charged. As a result, the composite film modified ITO electrode will be highly stable due to the electrostatic interactions between the positively charged nano TiO<sub>2</sub> and negatively charged PDDS. For comparison studies, PDDS film was electrodeposited on a bare ITO electrode surface in the same potential window following similar experimental conditions mentioned above.

## 3. Results and discussion

### 3.1. EQCM studies for the investigation of PDDS film growth process

In situ mass changes in nanogram range during electrochemical measurements could be monitored by EQCM technique [48]. EQCM studies provide valuable information about change in composition of species on the interface of a working electrode during conductive polymer redox switching processes. Furthermore, EQCM is also a versatile tool to substantiate polymer deposition from the corresponding mass changes during each potential cycle run [49]. In the present study, we utilized EQCM technique for monitoring the PDDS film growth process. Prior to conducting experiments, Au electrode surface in an AT-cut quartz crystal was cleaned well and immersed into TiO<sub>2</sub> nanoparticles/ethanol suspension for 20 min. After 20 min, thus obtained nano TiO<sub>2</sub> modified Au electrode was taken out, dried and gently washed with doubly distilled water and transferred into a Teflon cell containing 0.5 mM DDS in 0.1 M H<sub>2</sub>SO<sub>4</sub>. Then 20 consecutive CV potential scans were run in the potential

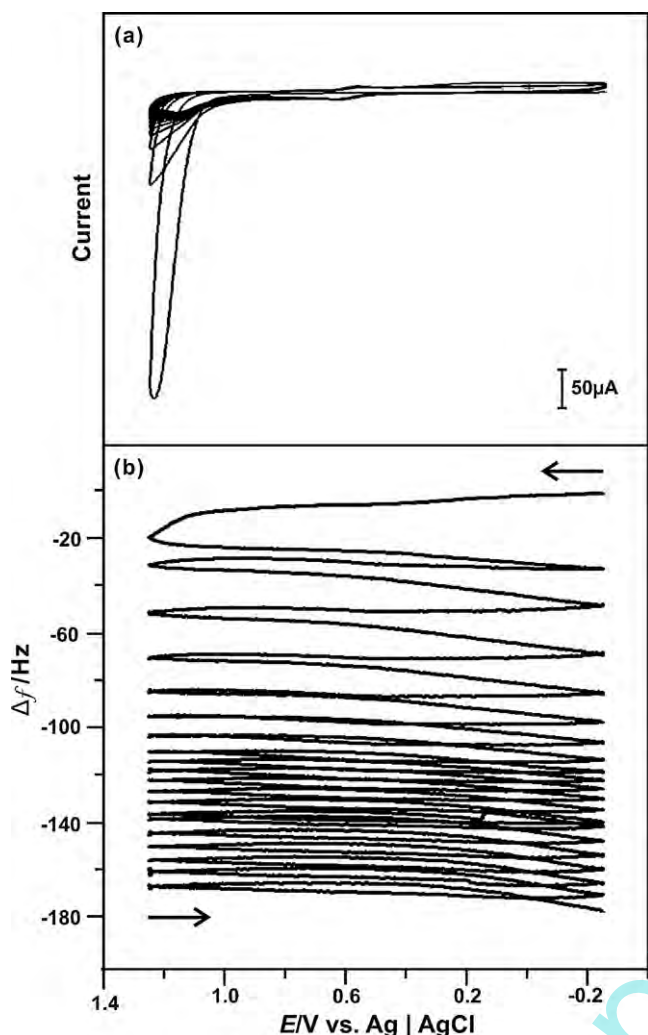


**Fig. 1.** (a) 20 consecutive cyclic voltammograms recorded at nano  $\text{TiO}_2$  film modified Au electrode kept in 0.5 mM DDS solution. The supporting electrolyte is 0.1 M  $\text{H}_2\text{SO}_4$ . Scan rate =  $100 \text{ mV s}^{-1}$ . (b) The corresponding EQCM frequency change observed for 20 consecutive cyclic voltammograms as that of (a).

range between  $-0.25$  and  $1.25 \text{ V}$  as shown in Fig. 1(a). When the potential was swept to more positive side, i.e.  $+1.25 \text{ V}$  the resonance frequency decreased for each cycle which indicates a continuous increase in mass above the crystal. Thus PDDS film growth was successfully occurred during each cycle. The frequency decrease corresponding to each PDDS film deposition cycle is shown in Fig. 1(b). From the frequency change, the mass change has been calculated using Sauerbrey equation [50,51]. Here,  $1 \text{ Hz}$  frequency change corresponds to  $1.4 \text{ ng cm}^{-2}$  of mass change. The total mass change after 20 PDDS film deposition cycles is  $243 \text{ ng cm}^{-2}$ .

### 3.2. Electrochemical behavior of various film modified ITO electrodes

The electrochemical behavior of nano  $\text{TiO}_2$ , bare, PDDS and PDDS/ $\text{TiO}_2$  modified ITO have been investigated using CV and the results are shown in Fig. 2. Cyclic voltammograms were recorded at the scan rate of  $50 \text{ mV s}^{-1}$  in  $\text{N}_2$  saturated 0.1 M  $\text{H}_2\text{SO}_4$  in the potential range between 0 and 0.9 V. Among the above said modified electrodes, nano  $\text{TiO}_2$  modified ITO exhibits a small redox couple as shown in Fig. 2(a). Its  $E_{\text{pa}}$  and  $E_{\text{pc}}$  values are 0.318 V and 0.138 V. However, no significant redox peaks were noticed at bare ITO (see Fig. 2(b)). In contrast, PDDS/ITO exhibits two redox couples with higher peak currents (see Fig. 2(c)). Their  $E_{\text{pa}}$  values

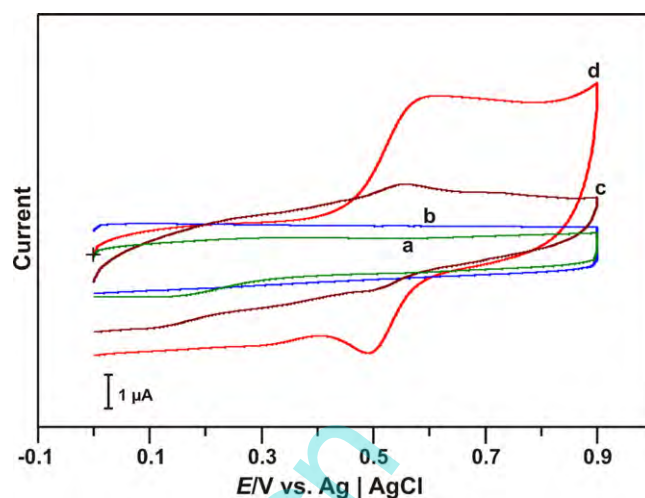


**Fig. 2.** Cyclic voltammograms recorded at (a) nano  $\text{TiO}_2$ , (b) bare, (c) PDDS, and (d) PDDS/ $\text{TiO}_2$  film modified ITO in  $\text{N}_2$  saturated 0.1 M  $\text{H}_2\text{SO}_4$ . Scan rate =  $50 \text{ mV s}^{-1}$ .

are 0.556 V and 0.245 V;  $E_{\text{pc}}$  values are 0.512 V and 0.120 V. The formal potential ( $E^{\circ'}$ ) values are 0.534 V and 0.183 V. Among all the above mentioned modified electrodes, PDDS/ $\text{TiO}_2$  composite film modified ITO electrode exhibits a well defined redox couple with maximum peak current as shown in Fig. 2(d). The  $E_{\text{pa}}$ ,  $E_{\text{pc}}$  and  $E^{\circ'}$  values are 0.614 V, 0.490 V and 0.552 V, respectively. Here, it is noteworthy that  $E^{\circ'}$  value of redox couple at the composite film is 18 mV positive than that of PDDS/ITO. The significant enhancement in redox peak currents along with positive shift in  $E^{\circ'}$  value at composite film could be attributed to the synergistic effect of PDDS incorporated  $\text{TiO}_2$  nanoparticles. Furthermore, surface coverage concentration ( $\Gamma$ ) results validate that more amount of PDDS have been efficiently deposited at the composite film. The  $\Gamma$  value of PDDS at PDDS/ $\text{TiO}_2$ /ITO and PDDS/ITO are  $1.37 \times 10^{-10} \text{ mol cm}^{-2}$  and  $2.21 \times 10^{-11} \text{ mol cm}^{-2}$  respectively. It is clear that  $\Gamma$  value observed at the composite film is 6.2-fold higher than that of PDDS film. The notable enhancement in  $\Gamma$  value at composite film could be attributed to the large surface area, porous nature and positive surface charge of  $\text{TiO}_2$  nanoparticles [47].

### 3.3. Different scan rate and pH studies

The effect of scan rates at PDDS/ $\text{TiO}_2$  composite film has been investigated in  $\text{N}_2$  saturated 0.1 M  $\text{H}_2\text{SO}_4$  using CV studies. The cyclic voltammograms are shown in Fig. 3.  $I_{\text{pa}}$  and  $I_{\text{pc}}$  increase linearly with increase in scan rates between 100 and  $1000 \text{ mV s}^{-1}$ . The different scan rate result illustrates that electron transfer process occurring at the composite film is a surface confined process. Fig. 3 inset shows the linear dependence of  $I_{\text{pa}}$  and  $I_{\text{pc}}$  with scan rates between 100 and  $1000 \text{ mV s}^{-1}$ .

The effect of pH on  $E^{\circ'}$  of PDDS/ $\text{TiO}_2$  composite film has been investigated using CV studies in  $\text{N}_2$  saturated different buffer solutions with pH 1, 4, 7 and 9. The results are shown in Fig. 4. It is clear from Fig. 4(a) that composite film exhibits a well defined reversible redox couple in pH 1. This shows the good stability of composite film in acidic pH. However, when composite film modified ITO electrode was transferred to different pH solutions, redox couple showed a steady potential shift with constant decrease in both anodic and cathodic peak currents (see Fig. 4(b)–(d)). The linear dependence of  $E^{\circ'}$  of composite film with pH is shown in Fig. 4 inset. The slope value of  $E^{\circ'}$  vs. pH is observed to be  $56 \text{ mV pH}^{-1}$ , which is close to the theoretical slope value of  $59 \text{ mV pH}^{-1}$  for equal number of proton and electron transfer process.

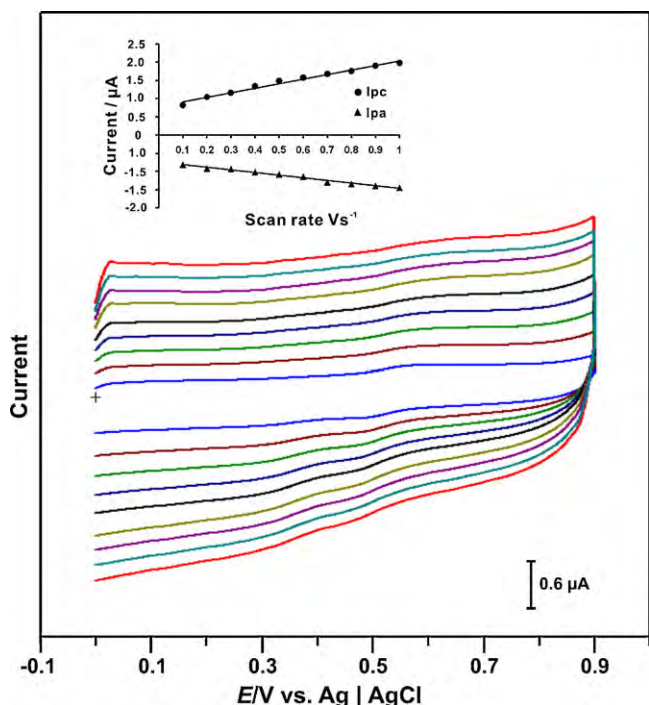


**Fig. 3.** Cyclic voltammograms recorded at PDDSS/TiO<sub>2</sub> composite film in N<sub>2</sub> saturated 0.1 M H<sub>2</sub>SO<sub>4</sub> at different scan rates. The scan rates from inner to outer are: 100, 200, 300, 400, 500, 600, 700, 800, 900 and 1000 mV s<sup>-1</sup>. Inset shows the linear dependence of  $I_{pa}$  and  $I_{pc}$  on scan rates between 100 and 1000 mV s<sup>-1</sup>.

#### 3.4. Surface morphological characterizations using SEM, AFM and XRD studies

Fig. 5 shows top and 3D view of SEM and AFM images of PDDSS, nano TiO<sub>2</sub> and PDDSS/TiO<sub>2</sub> film modified ITO electrodes. The top view SEM image of PDDSS film demonstrates thin polymer film coated ITO electrode surface. Where, several flattened small PDDSS globular structures have been randomly distributed. In contrast,

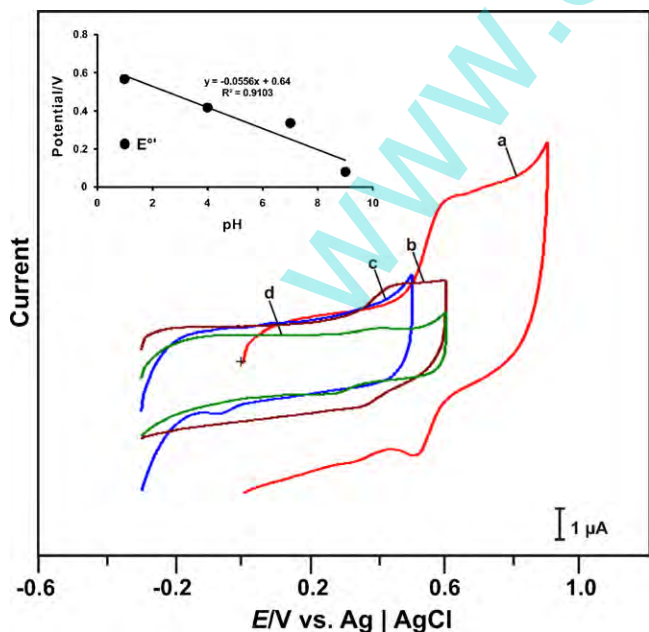


**Fig. 4.** Cyclic voltammograms obtained at PDDSS/TiO<sub>2</sub> composite film in N<sub>2</sub> saturated different buffer solutions with pH (a) 1, (b) 4, (c) 7, and (d) 9. Scan rate = 50 mV s<sup>-1</sup>. Inset shows influence of pH on the  $E^{\circ'}$  of PDDSS/TiO<sub>2</sub> composite film.

3D AFM image of PDDSS film surface shows random distribution of slightly elongated PDDSS globules with variable sizes. This result illustrates that PDDSS film growth is not efficient on the bare ITO electrode surface. On the other hand, SEM image of nano TiO<sub>2</sub> film possess numerous granular TiO<sub>2</sub> nanoparticles which are closely distributed throughout the ITO electrode surface. Similarly, the AFM image of nano TiO<sub>2</sub> film also illustrates the presence of granular TiO<sub>2</sub> nanoparticles. The size of TiO<sub>2</sub> nanoparticles was between 130 and 180 nm. On the other hand, SEM image of PDDSS/TiO<sub>2</sub> composite film depicts much uniform surface morphology. The TiO<sub>2</sub> nanoparticles are not clearly seen since they are covered well by the PDDSS film. Likewise, AFM image of composite film also shows several PDDSS coated TiO<sub>2</sub> nanoparticles formed on the ITO electrode surface. The uniform surface morphology of composite film could be attributed to the efficient loading of PDDSS globules in to porous TiO<sub>2</sub> matrix. This result validates that nano TiO<sub>2</sub> modified ITO electrode surface is more efficient for PDDSS film growth. From AFM data, the average surface roughness values of PDDSS, nano TiO<sub>2</sub> and PDDSS/TiO<sub>2</sub> composite films have been calculated. They are 30.2, 1.84 and 7.21 nm respectively. It was apparent that average surface roughness value of the composite film is 3.9-fold higher than that of only nano TiO<sub>2</sub> film and 4.2-fold lower than that of PDDSS film. The notable enhancement in average surface roughness value at composite film than nano TiO<sub>2</sub> film confirms the formation of PDDSS coating on TiO<sub>2</sub> nanoparticles, while the decrease in average surface roughness value of composite film than PDDSS film shows its smooth surface morphology.

In order to ascertain the crystalline nature of TiO<sub>2</sub> nanoparticles, X-ray diffraction (XRD) studies have been performed. Fig. 6 shows the XRD pattern of TiO<sub>2</sub> nanoparticles used in this work. The results reveal that diffraction peaks seen in the XRD pattern of TiO<sub>2</sub> nanoparticles correspond to anatase phase and they have good crystalline nature. The peak positions and their relative intensities are consistent with standard powder diffraction pattern of anatase reported earlier [52,53].

#### 3.5. EIS and light induced EIS studies at different film modified ITO electrodes

EIS measurements were carried out in the absence of light at bare, nano TiO<sub>2</sub>, PDDSS and PDDSS/TiO<sub>2</sub> composite film modified ITO electrodes and the results are shown in Fig. 7(a). The supporting electrolyte used was 0.1 M H<sub>2</sub>SO<sub>4</sub> containing 5 mM Fe(CN)<sub>6</sub><sup>3-/4-</sup>. Inset represents Randles equivalence circuit model used to fit the experimental data. Where,  $R_s$  represents electrolyte resistance,  $R_{et}$  charge transfer resistance,  $C_{dl}$  double layer capacitance and  $Z_w$  Warburg impedance. The  $R_{et}$  and  $C_{dl}$  values calculated for all the above-mentioned electrodes are given in Table 1. Generally, semicircle portion observed at higher frequencies in a Nyquist plot corresponds to electron-transfer-limited process and diameter of the semicircle corresponds to interfacial electron-transfer resistance ( $R_{et}$ ). Linear part of the spectrum is characteristic of lower frequency range and represents diffusional-limited process [54,55]. In Fig. 7(a), an enlarged semicircle portion is observed at PDDSS film modified ITO. Its  $R_{et}$  value is 560 Ω (see Table 1). This result indicates that PDDSS film exhibits a substantial hindrance to electron transfer. On the other hand, the Nyquist plots of bare, nano TiO<sub>2</sub> and PDDSS/TiO<sub>2</sub> composite film modified ITO exhibit much depressed semicircles. Their  $R_{et}$  values are 330 Ω, 240 Ω and 170 Ω respectively (see Table 1). Among all the above mentioned ITO, smallest semicircle diameter with much lower  $R_{et}$  value (170 Ω) has been observed at the composite film modified ITO which ultimately reveals a rapid electron transfer process. Thus incorporation of PDDSS with TiO<sub>2</sub> nanoparticles leads to good conductivity and rapid electron shuttling between the composite film and underlying electrode surface.

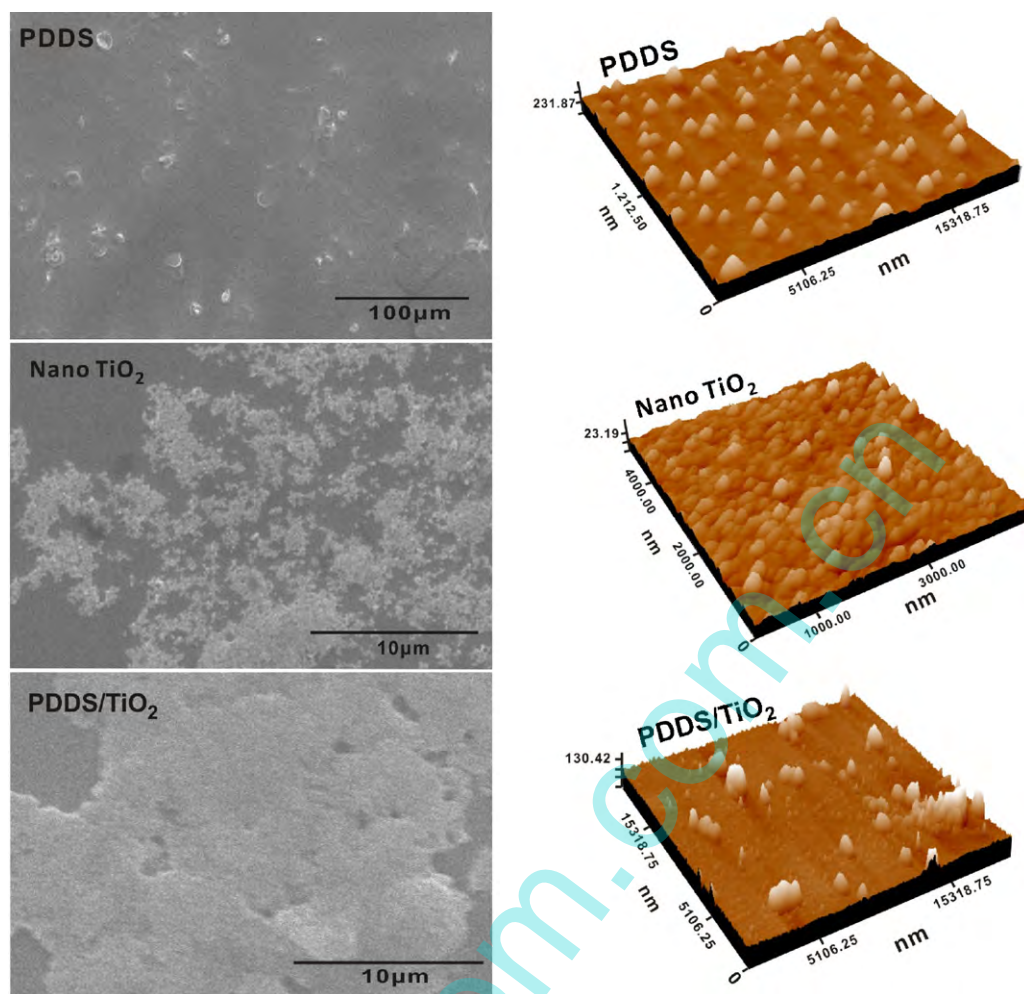


Fig. 5. Top view and 3D view of SEM and AFM images of PDDDS, nano TiO<sub>2</sub> and PDDDS/TiO<sub>2</sub> film modified ITO.

In addition, light induced EIS measurements have been conducted at bare, nano TiO<sub>2</sub>, PDDDS and PDDDS/TiO<sub>2</sub> composite film modified ITO in 0.1 M H<sub>2</sub>SO<sub>4</sub> containing 5 mM Fe(CN)<sub>6</sub><sup>3-/4-</sup>. Prior to EIS measurements, these ITO were subjected to 5 min irradiation (optimized time) and then Nyquist plots were recorded. The results are shown in Fig. 7(b). The  $R_{et}$  values of the above mentioned electrodes are given in Table 1. It is apparent from Fig. 7(b) and Table 1 that PDDDS/TiO<sub>2</sub> composite film possesses a much depressed semicircle and smallest  $R_{et}$  value than bare, nano TiO<sub>2</sub> and PDDDS films. It is noteworthy that  $R_{et}$  value of the composite film is 2.1-, 1.3- and 14.3-fold smaller than that of bare, nano TiO<sub>2</sub> and PDDDS films. Photo induced EIS results thus corroborates that among all the above-mentioned electrodes, composite film surface demonstrates maximum photosensitivity and it drastically promotes the rapid electron transfer process upon irradiation. Furthermore, effect of irradiation time on the impedance behavior of composite film has also been investigated using EIS studies. Nyquist plots obtained at composite film for various irradiation times such as 30 s, 1 min, 2 min and 5 min are shown in Fig. 7(c). The corresponding  $R_{et}$  values are presented in Table 2. The semicircle diameter and  $R_{et}$  values of the composite film increase linearly with increase in irradiation time (up to 5 min). However, there has been no notable increase in capacitance values. Thus composite film surface is highly photo sensitive for 5 min irradiation and this optimized irradiation time has been used for the photoelectrocatalytic experiments.

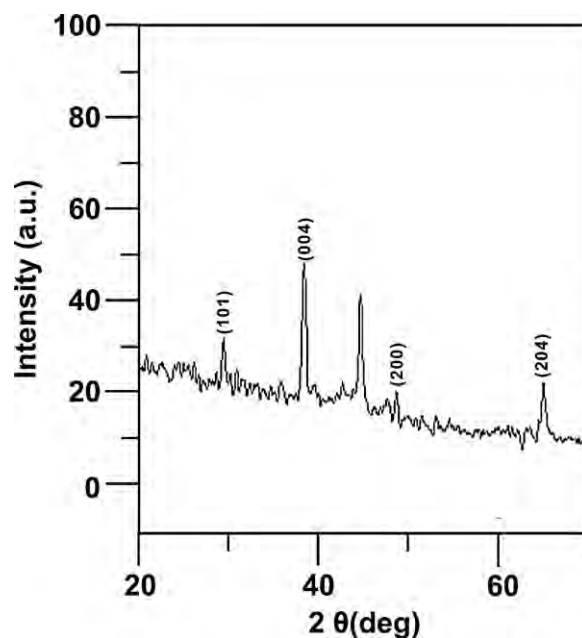


Fig. 6. XRD pattern of TiO<sub>2</sub> nanoparticles.

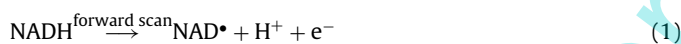
**Table 1**

$R_{et}$  and  $C_{dl}$  values obtained at different film modified ITO both before and after 5 min irradiation of the electrode surfaces.

Film type	Before irradiation		After 5 min irradiation	
	Electron transfer resistance, $R_{et}$ ( $\Omega$ )	Double layer capacitance, $C_{dl}$ ( $\mu\text{F}$ )	Electron transfer resistance, $R_{et}$ ( $\Omega$ )	Double layer capacitance, $C_{dl}$ ( $\mu\text{F}$ )
Bare	330	14.03	1180	5.61
Nano TiO <sub>2</sub>	240	16.64	740	7.10
PDDS	560	20.5	7980	20.09
PDDS/TiO <sub>2</sub>	170	26.64	560	26.71

### 3.6. Investigation of electrocatalytic regeneration of NADH at various modified ITO electrodes

Fig. 8(a)–(d) represents cyclic voltammograms obtained at bare, nano TiO<sub>2</sub>, PDDS and PDDS/TiO<sub>2</sub> modified ITO electrodes in the presence of 0.12  $\mu\text{M}$  NADH in N<sub>2</sub> saturated 0.1 M H<sub>2</sub>SO<sub>4</sub>. The potential range employed for electrocatalytic studies is between –0.1 and 0.5 V. As shown in Fig. 8(a) and (b), no significant anodic peaks were observed at both bare and nano TiO<sub>2</sub> modified ITO electrodes in this potential range. However, during forward potential scan, PDDS/ITO exhibits a small anodic peak at 0.275 V (see Fig. 8(c)). During the reverse scan no cathodic peak was observed. In contrast, PDDS/TiO<sub>2</sub> composite film modified ITO exhibits an enhanced anodic peak at 0.267 V in forward scan and a well defined cathodic peak at 0.095 V in reverse scan (see Fig. 8(d)). Moreover, anodic peak current noticed at the composite film was 18-fold higher than that of PDDS film. The great enhancement in anodic peak current observed at composite film shows its promising electrocatalytic activity towards NADH. Similarly, well defined cathodic peak observed at composite film validates the regeneration of NADH as explained by following mechanism. The possible mechanism for regeneration of NADH at composite film surface has been explained below:



In the above NADH oxidation pathway, oxidation of NADH in the forward scan might result in the formation of NAD<sup>•</sup> which could be accompanied by the release of an e<sup>–</sup> and one H<sup>+</sup> as illustrated in Eq. (1). However, there is no direct electrochemical evidence available in the literature for neutral radical NAD<sup>•</sup> formation. Therefore, we are not able to conclude the neutral radical NAD<sup>•</sup> formation from CV results alone and considerable uncertainty exists in the reaction pathway. On the other hand, Grodkowski et al. have investigated the one-electron transfer reactions involving the couple NAD<sup>•</sup>/NADH in aqueous solutions using pulse radiolysis [56]. They confirmed from their experimental results that one electron oxidation of NADH are rather slow than similar reactions which are driven by a similar redox potential difference. They reported a potential of  $E = +0.30$  V vs. NHE for the couple NAD<sup>•</sup>/NADH. Similarly, Umrikhina et al. confirmed the NADH and NADPH free radicals (NAD<sup>•</sup> and NADPH<sup>•</sup>) formation when NADH aqueous solution was irradiated by UV light (340 nm) [57]. Although the above mentioned studies confirm the possibility of NAD<sup>•</sup> formation, there is always uncertainty in its formation in the NADH reaction pathway due to its shorter life time. Therefore we believe that the oxidation

of NADH in the present study could follow an alternative NADH oxidation mechanism [58].



In the above mechanism, radical cation formation occurs in the first step (Eq. (3)), followed by the deprotonation of radical cation to NAD<sup>•</sup> (Eq. (4)). As reported earlier by Zhu et al. the proton transfer from the radical cation in Eq. (4) should be extremely fast and possibly diffusion controlled in aqueous solution which they confirmed from the very low heterolytic bond dissociation energy (5.1 kcal/mol) calculated for NADH<sup>•+</sup> [59]. NAD<sup>•</sup> produced in Eq. (4) should be immediately converted to NAD<sup>+</sup> at the electrode surface as shown in Eq. (5).

### 3.7. UV-vis absorption spectroscopy study as an evidence for the conversion of NADH/NAD<sup>+</sup> in NADH oxidation reaction pathway

As reported earlier, UV-vis absorption spectroscopy can be used as an effective tool to confirm the conversion of NADH to NAD<sup>+</sup> [60]. Aqueous solution of NADH exhibits two absorption maxima at 260 nm and 340 nm [61]. Where, the absorption band at 260 nm corresponds to the adenine ring and the other at 340 nm arises due to the reduced nicotinamide ring. On the other hand, UV-vis absorption spectrum of NAD<sup>+</sup> possesses only a single absorption band at 260 nm [62]. Since we prepared the NADH solutions using 0.1 M H<sub>2</sub>SO<sub>4</sub> in the present study, the characteristic absorption band at 340 nm is rapidly lost at acidic pH and it has been replaced by an absorbance band at 290 nm. This shift is due to a transience directly related to acidity [63]. As a result, we observed two characteristic absorption bands at 240 and 290 nm in the UV-vis absorption spectra of 20 nM NADH solution recorded in the wavelength range between 200 and 600 nm. The intensity of these absorption bands increased linearly with increase in NADH concentration between 20 nM and 41 nM. In order to confirm the conversion of NADH/NAD<sup>+</sup>, UV-visible absorption spectra were recorded before and after performing repeated square wave voltammograms (SWVs) at PDDS/TiO<sub>2</sub> modified ITO in 20 nM to 41 nM NADH solution. The results show that the absorption spectra of NADH recorded without performing SWVs exhibits two characteristic absorption bands at 240 and 290 nm. Whereas the absorption spectra of NADH recorded after performing repeated SWVs possess only a single absorption band at 240 nm, i.e. the absorption band at 290 nm disappeared. Further, the intensity of the absorption band ( $A_{240}$ ) increased with increase in NADH concentration. Comparing Fig. 9(c) with (b) it

**Table 2**

$R_{et}$  and  $C_{dl}$  values obtained at PDDS/TiO<sub>2</sub> composite film modified ITO electrode after different irradiation time intervals.

Film type	Electron transfer resistance, $R_{et}$ ( $\Omega$ ) for various irradiation time intervals				Double layer capacitance, $C_{dl}$ ( $\mu\text{F}$ ) for various irradiation time intervals			
	30 s	1 min	2 min	5 min	30 s	1 min	2 min	5 min
PDDS/TiO <sub>2</sub>	240	290	380	560	26.63	26.68	26.73	26.71

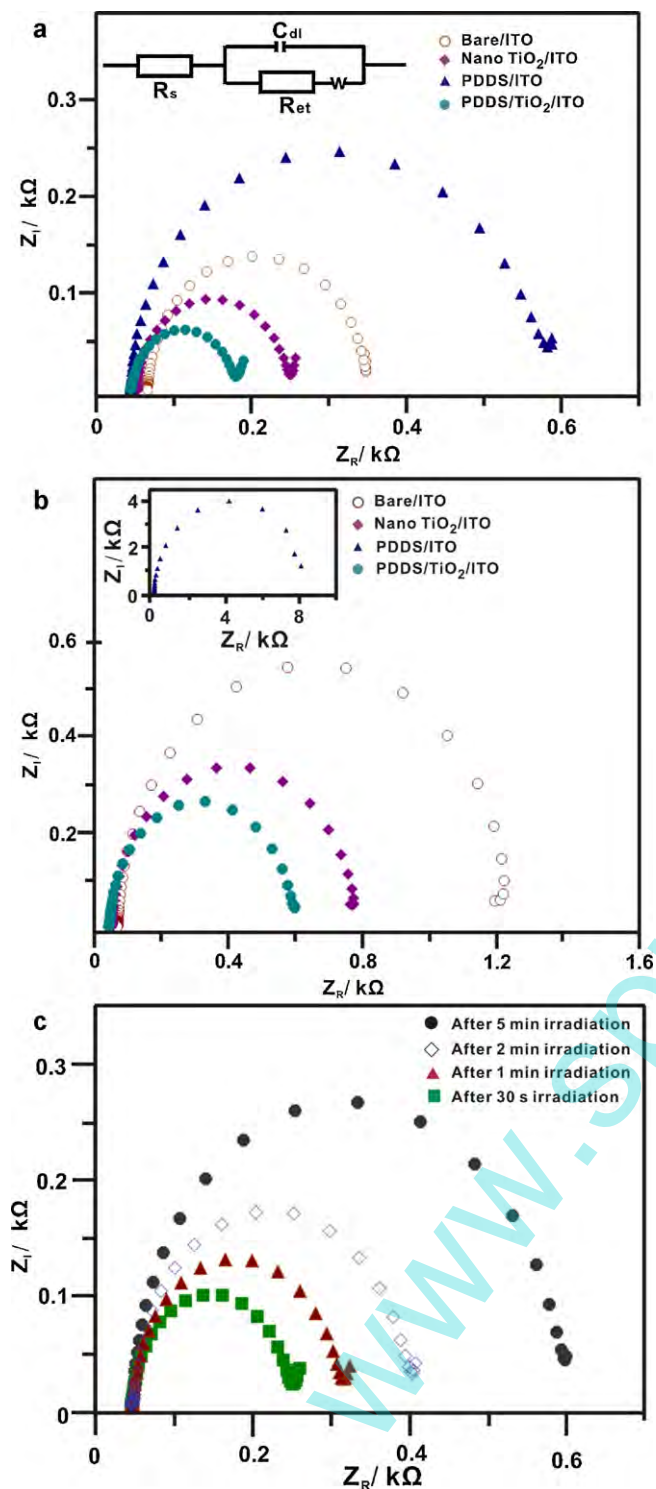


Fig. 7. EIS of bare, nano  $\text{TiO}_2$ , PDDDS and PDDDS/ $\text{TiO}_2$  composite film modified ITO obtained (a) without and (b) with 5 min irradiation in 0.1 M  $\text{H}_2\text{SO}_4$  containing 5 mM  $\text{Fe}(\text{CN})_6^{3-/4-}$ ; frequency: 0.1 Hz to 100 kHz. Insets are: (a) Randles circuit for all the above-mentioned electrodes and (b) EIS of PDDDS film modified ITO electrode obtained after 5 min irradiation. (c) EIS of PDDDS/ $\text{TiO}_2$  composite film modified ITO electrode recorded with 30 s, 1, 2 and 5 min irradiation.

is obvious that the intensity of absorption band ( $A_{240}$ ) obtained in 33 nM NADH solution is higher than that obtained in 29 nM NADH. Thus the appearance of single absorption band ( $A_{240}$ ) and the augmentation of its intensity with NADH concentration increments confirm the conversion of NADH/ $\text{NAD}^+$ . Vijaya et al. reported a

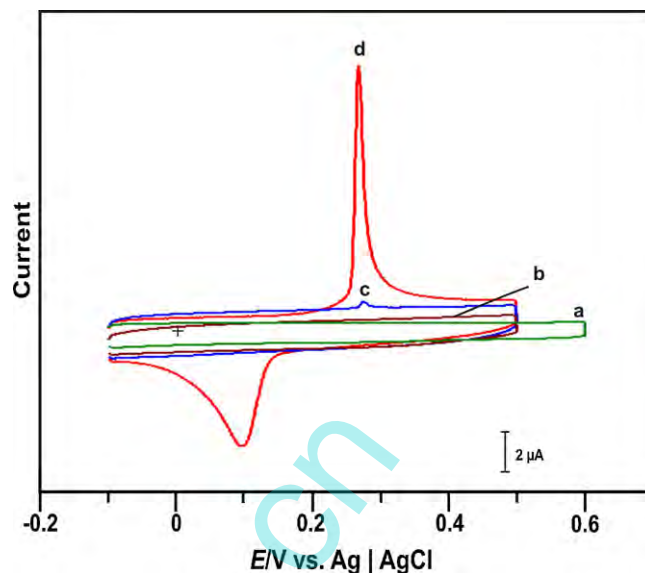


Fig. 8. Cyclic voltammograms recorded at (a) bare, (b) nano  $\text{TiO}_2$ , (c) PDDDS, and (d) PDDDS/ $\text{TiO}_2$  composite film modified ITO in the presence of  $0.12 \mu\text{M}$  NADH in  $\text{N}_2$  saturated 0.1 M  $\text{H}_2\text{SO}_4$ . Scan rate =  $50 \text{ mV s}^{-1}$ .

similar UV–visible absorption band ( $A_{240}$ ) for Vanadate stimulated oxidation of NADH [64]. They confirmed from UV–vis absorption results that oxidation of NADH was accompanied by an increase in absorbance at 240 nm, and the spectrum of the reaction mixture showed a peak at 240 nm which increased with time. Further, the mechanism for NADH oxidation proposed by Vijaya et al. involves the formation of  $\text{NAD}^{\bullet}$  free radical by the interaction of NADH with  $\text{V}^{\text{V}}$  in the first step which is followed by the reaction of  $\text{NAD}^{\bullet}$  with oxygen to give  $\text{NAD}^+$  and  $\text{O}_2^-$ , which then gives rise to  $\text{H}_2\text{O}_2$ . UV–vis absorption spectroscopy results obtained in the present study are thus in good agreement with the previous results available in literature and it provides an evidence for the conversion of NADH/ $\text{NAD}^+$ .

### 3.8. Optimization of irradiation time and investigation of photoelectrocatalytic regeneration of NADH at PDDDS/ $\text{TiO}_2$ modified ITO electrodes

Owing to the excellent electrocatalytic ability of composite film towards NADH we have carried out photoelectrocatalytic NADH regeneration studies. Photoelectrocatalytic experiments were car-

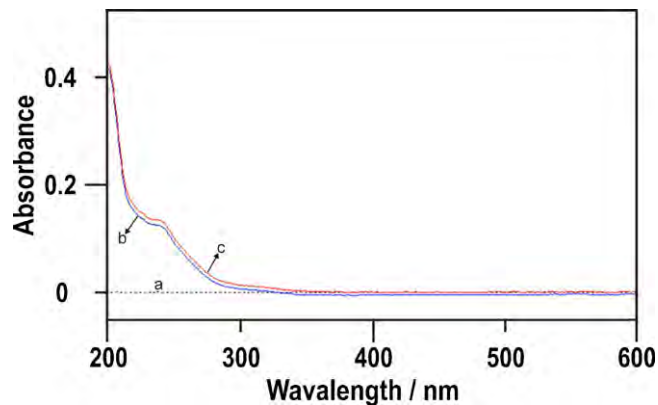
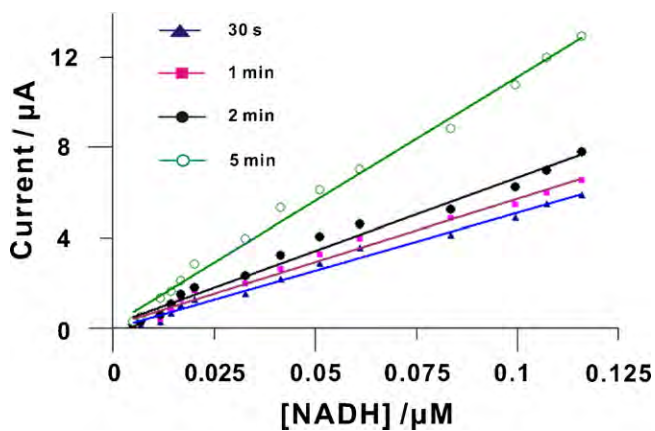


Fig. 9. UV–vis spectra of (a) blank solution, (b) 29 nM, and (c) 33 nM NADH solutions recorded after performing repeated SWVs at the composite film in the potential range between  $-0.1$  and  $0.5 \text{ V}$ . Supporting electrolyte: 0.1 M  $\text{H}_2\text{SO}_4$ . The characteristic absorption peak observed at 240 nm in (b) and (c) confirms the conversion of NADH/ $\text{NAD}^+$ .



**Fig. 10.** The irradiation time optimization plot of PDDs/TiO<sub>2</sub> composite film; irradiation time intervals used were: 30 s (filled triangle), 1 min (filled square), 2 min (filled circle) or 5 min (unfilled circle); cyclic voltammograms were recorded at the irradiated composite film ITO electrode at the scan rate of 50 mV s<sup>-1</sup> in N<sub>2</sub> saturated 0.1 M H<sub>2</sub>SO<sub>4</sub> containing 0.005–0.12 μM NADH.

ried out using a light emitting diode (WLL01) with an average intensity of 63.581u (W/m<sup>2</sup>). A normalized intensity/Volt of 1 (WV<sup>-1</sup> m<sup>-2</sup>) 472, 25 (nm, Δnm) was employed throughout the photoelectrocatalytic experiments. Initially, composite film irradiation time was optimized and the results are shown in Fig. 10. Prior to each NADH concentration addition, composite film surface was irradiated for 30 s, 1 min, 2 min or 5 min and the light source was turned off immediately. Then aliquots of NADH were sequentially added into N<sub>2</sub> saturated 0.1 M H<sub>2</sub>SO<sub>4</sub> and cyclic voltammograms were recorded. From the obtained cyclic voltammograms photoelectrocatalytic anodic currents were measured and plotted against [NADH]/μM as shown in Fig. 10. It is clear that the photoelectrocatalytic NADH oxidation current generated at composite film increases linearly with increase in irradiation time and sequential NADH concentration additions. The sensitivity values obtained at the composite film for 30 s, 1 min, 2 min and 5 min irradiation are 58.5, 63.0, 64.9 and 109.7 μA μM<sup>-1</sup> of NADH. The correlation coefficients are 0.984, 0.989, 0.983 and 0.994 respectively. Since maximum photoelectrocatalytic response and higher sensitivity has been observed at the composite film for 5 min irradiation, we have utilized this optimized time for all photoelectrocatalytic experiments.

Fig. 11(a) and (b) shows the cyclic voltammograms recorded at composite film before and after 5 min irradiation in the presence of 0.005 μM NADH. Similarly, Fig. 11(c) and (d) represents cyclic voltammograms recorded at the composite film in the presence of 0.12 μM NADH as similar conditions as that of (a) and (b). The well defined photoelectrocatalytic peaks with maximum  $I_{pa}$  and  $I_{pc}$  have been observed at the composite film surface for 5 min irradiation. However, even after 5 min irradiation no significant photoelectrocatalytic peaks was noticed at bare ITO even in the presence of 0.12 μM NADH (see Fig. 11(e)). This result confirms that photoelectrocatalytic NADH regeneration ability of the composite film is much higher than that of bare ITO. It could be attributed to the presence of highly photosensitive TiO<sub>2</sub> nanoparticles layer and the synergistic effect of PDDs/TiO<sub>2</sub> composite towards NADH. Fig. 11 inset plot shows linear dependence of peak currents observed at composite film before and after 5 min irradiation with sequential NADH concentration additions in the concentration range between 0.005 and 0.12 μM. The sensitivity and correlation coefficient values are 86.5 μA μM<sup>-1</sup> and 124.1 μA μM<sup>-1</sup> of NADH and 0.995 and 0.996 respectively. Maximum sensitivity has been obtained at the composite film after 5 min irradiation which corroborates its excellent photoelectrocatalytic regeneration ability for NADH.

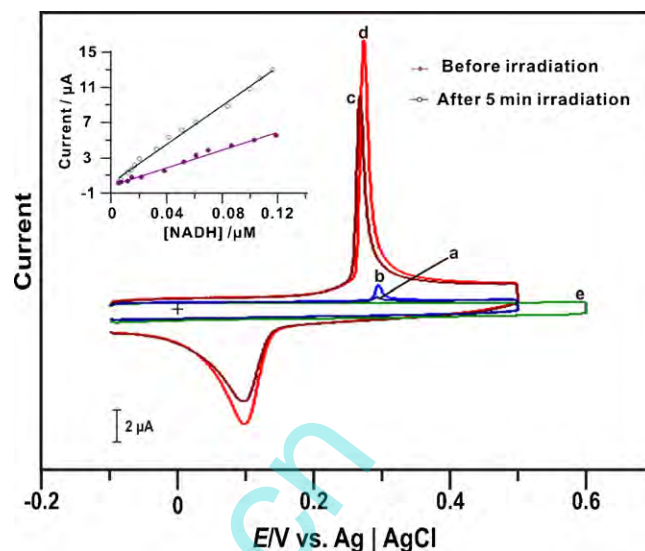
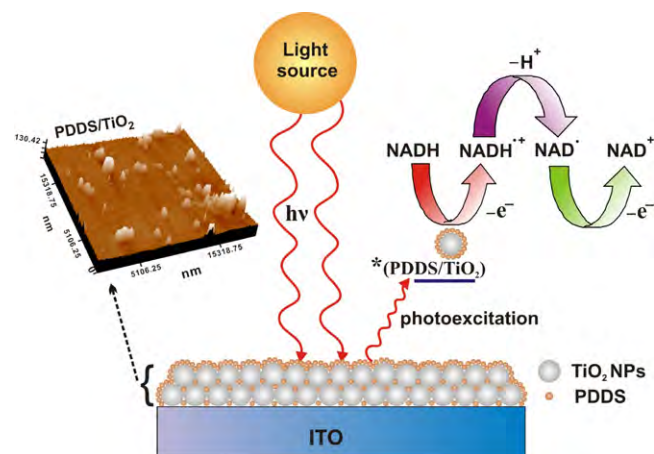


**Fig. 11.** Cyclic voltammograms recorded before (a) and after 5 min irradiation (b) of the PDDs/TiO<sub>2</sub> composite film in 0.005 μM NADH; (c) and (d) were obtained at similar conditions as that of (a) and (b) but in presence of 0.12 μM NADH. (e) 5 min irradiated bare ITO kept in 0.12 μM NADH. Scan rate: 50 mV s<sup>-1</sup>; supporting electrolyte: N<sub>2</sub> saturated 0.1 M H<sub>2</sub>SO<sub>4</sub>. Inset is the plot of photoelectrocatalytic NADH oxidation peak current (without/with 5 min irradiation) vs. [NADH]; [NADH] range used: 0.005–0.12 μM, respectively.

The linear concentration range is between 0.022 and 0.12 μM NADH respectively. In addition, we have also explained the mechanism of photoelectrocatalytic regeneration of NADH at PDDs/TiO<sub>2</sub> composite film modified ITO electrode in Scheme 1. As demonstrated in Scheme 1, irradiation of the PDDs/TiO<sub>2</sub> composite film surface leads to photoexcitation. Upon NADH addition, photoexcited \*(PDDs/TiO<sub>2</sub>) composite film surface notably triggers the oxidation of NADH which involves the conversion of NADH/NAD<sup>+</sup> accompanied by 2e<sup>-</sup> and H<sup>+</sup> transfer. Dilgin et al. [40] and Stigor et al. [41] reported similar photoelectrocatalytic excitation step for NADH oxidation at poly (Toluidine Blue O) and polyphenothiazine formaldehyde modified matrices.

### 3.9. Square wave voltammetry (SWV) studies

SWV studies have been performed before and after 5 min irradiation at PDDs/TiO<sub>2</sub> composite film modified ITO in 0.1 M H<sub>2</sub>SO<sub>4</sub> solution. The potential range was -0.1 V to 0.5 V. Fig. 12(a)–(g) dis-



**Scheme 1.** The possible mechanism for photoelectrocatalytic NADH regeneration at the PDDs/TiO<sub>2</sub> composite film modified ITO.

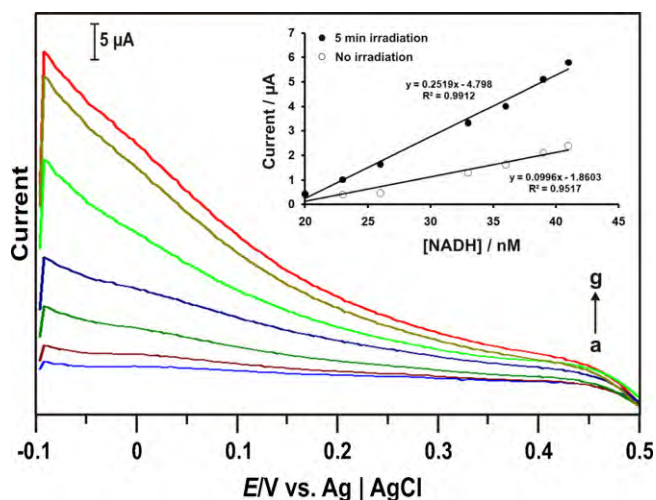


**Fig. 12.** Background subtracted SWVs recorded at 5 min irradiated PDDs/TiO<sub>2</sub> composite film in the presence of (a) 20 nM, (b) 23 nM, (c) 26 nM, (d) 33 nM, (e) 36 nM, (f) 39 nM, and (g) 41 nM NADH. Supporting electrolyte: 0.1 M H<sub>2</sub>SO<sub>4</sub>; frequency: 15 Hz. Inset is the plot of photoelectrocatalytic NADH oxidation peak current (with/without 5 min irradiation) vs. [NADH]; [NADH] used: 20–41 nM, respectively.

play the background subtracted SWVs obtained at PDDs/TiO<sub>2</sub>/ITO after 5 min irradiation with increasing NADH concentrations from 20 nM to 41 nM. The calibration plot shown in Fig. 12 inset shows that the NADH oxidation peak current observed at irradiated composite film surface is several folds higher than that obtained without irradiation and it increases linearly with increase in NADH concentration additions. From the calibration plot of the irradiated composite film, the linear concentration range is obtained as 23 and 39 nM NADH. The sensitivity is about 0.252  $\mu\text{A nM}^{-1}$ , respectively. Further, the sensitivity of the composite film with irradiation is higher than the sensitivity obtained without irradiation, i.e. 0.099  $\mu\text{A nM}^{-1}$ . Thus SWV results validate the good photoelectrocatalytic efficiency of the irradiated composite film towards NADH oxidation.

### 3.10. Repeatability, reproducibility and interference studies

SWV technique has been used to investigate the repeatability, reproducibility and selectivity of the proposed method. Prior to recording SWVs, PDDs/TiO<sub>2</sub> composite film surface was irradiated for 5 min and its photoelectrocatalytic response towards 33 nM (within the working linear range) was investigated in 0.1 M H<sub>2</sub>SO<sub>4</sub> supporting electrolyte solution. The relative standard deviation (RSD) for six repetitive NADH measurements is 3.4% which validate the good repeatability of the proposed method. Furthermore, in order to ascertain the reproducibility of the proposed method, three composite films modified ITO have been prepared and their surfaces were irradiated for 5 min. The photoelectrocatalytic response of all three composite film electrodes towards 33 nM NADH was examined using SWV technique. From the obtained SWVs,  $I_{pa}$  values of NADH noticed at all three composite film modified ITO electrodes have been calculated and their relative standard deviation (RSD) is 4.8%. This result reveals the good reproducibility of the composite film for photoelectrocatalytic NADH oxidation.

In the present study, selectivity of the irradiated PDDs/TiO<sub>2</sub> composite film surface towards NADH was investigated in the presence of common interferences like ascorbic acid (AA), dopamine (DA) and uric acid (UA). Fig. 13(a) represents the square wave voltammogram obtained at the irradiated composite film surface in the absence of NADH. Whereas, Fig. 13(b) shows the square wave voltammogram obtained at the composite film in presence of 33 nM NADH. Comparing Fig. 13(b) with (a) it is clear that the

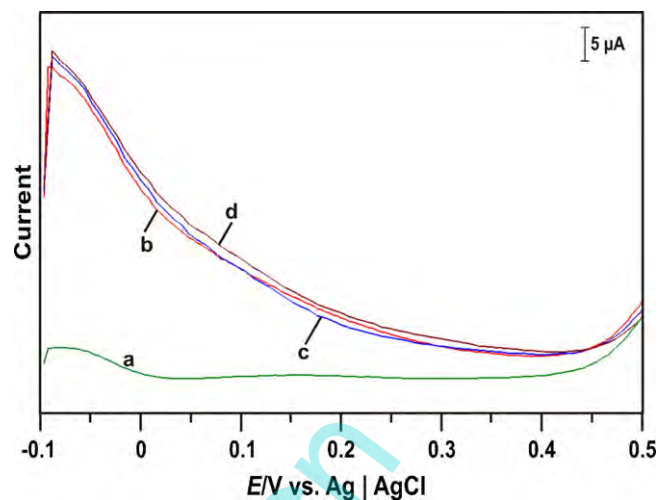


**Fig. 13.** SWVs recorded at 5 min irradiated PDDs/TiO<sub>2</sub> composite film in 0.1 M H<sub>2</sub>SO<sub>4</sub> containing (a) no NADH, (b) 33 nM NADH, (c) 33 nM NADH along with 3.3  $\mu\text{M}$  each AA, DA, UA (100-fold), and (d) 33 nM NADH along with 6.6  $\mu\text{M}$  each AA, DA and UA (200-fold) frequency: 15 Hz.

irradiated composite film exhibits an enhanced photoelectrocatalytic response towards 33 nM NADH. On the other hand, no characteristic anodic peaks of AA, DA or UA appeared in this potential range even when their concentration was 100-fold higher, i.e. 3.3  $\mu\text{M}$  of these interfering species coexist with 33 nM of NADH in the same supporting electrolyte solution (see Fig. 13(c)). Further, no notable change in the  $I_{pa}$  value of the composite film was observed. Similarly, as shown in Fig. 13(d) even when the AA, DA and UA concentration was increased 200-fold higher (6.6  $\mu\text{M}$ ) no characteristic peaks corresponding to the interfering species appeared. However, a marginal increase in the  $I_{pa}$  value was observed. This result indicates that composite film is highly selective towards NADH detection. The good selectivity of the composite film could be attributed to the repulsion between the negatively charged PDDs layer and negatively charged interfering species. As a result of this repulsive force, the diffusion rate of the interfering species towards the electrode surface could be much slower and thereby less interference effect will be produced.

## 4. Conclusions

We investigated the photoelectrocatalytic regeneration of NADH at PDDs/TiO<sub>2</sub> composite film modified ITO. Irradiation of composite film surface for 5 min produced significant enhancement in the NADH photocatalytic oxidation current. The photoelectrocatalytic regeneration ability of composite film is notably higher than that of only PDDs, nano TiO<sub>2</sub> and bare ITO electrodes. Further, the composite film showed good photocatalytic activity, rapid response towards NADH with good linear range and it possesses good selectivity for NADH. Since the proposed PDDs/TiO<sub>2</sub> composite is highly photosensitive it could be used as a novel platform to investigate the photoelectrocatalytic regeneration pathway of some vital biomolecules.

## Acknowledgements

This work was supported by the National Science Council and the Ministry of Education of Taiwan (Republic of China).

## References

- [1] J. Gebicki, A. Marcinek, J. Zielonka, Transient species in the stepwise interconversion of NADH and NAD<sup>+</sup>, *Acc. Chem. Res.* 37 (2004) 379–386.

- [2] J. Zen, A. Senthil Kumar, D. Tsai, Recent updates of chemically modified electrodes in analytical chemistry, *Electroanalysis* 15 (2003) 1073–1087.
- [3] J. Moiroux, P.J. Elving, Mechanistic aspects of the electrochemical oxidation of dihydronicotinamide adenine dinucleotide (NADH), *J. Am. Chem. Soc.* 102 (1980) 6533–6538.
- [4] A. Kitani, L.L. Miller, Fast oxidants for NADH and electrochemical discrimination between ascorbic acid and NADH, *J. Am. Chem. Soc.* 103 (1981) 3595–3597.
- [5] C.R. Raj, B.K. Jena, Efficient electrocatalytic oxidation of NADH at gold nanoparticles self-assembled on three-dimensional sol–gel network, *Chem. Commun.* (2005) 2005–2007.
- [6] B.F.Y.Y. Hin, C.R. Lowe, Catalytic oxidation of reduced nicotinamide adenine dinucleotide at hexacyanoferrate-modified nickel electrodes, *Anal. Chem.* 59 (1987) 2111–2115.
- [7] P.J. Eking, W.T. Bresnahan, J. Moiroux, Z. Samec, NAD/NADH as a model redox system: mechanism, mediation, modification by the environment, *Bioelectrochem.* 9 (1982) 365.
- [8] P. Ramesh, P. Sivakumar, S. Sampath, Phenoxazine functionalized, exfoliated graphite based electrodes for NADH oxidation and ethanol biosensing, *Electroanalysis* 15 (2003) 1850–1858.
- [9] F. Ricci, A. Amine, D. Moscone, G. Palleschi, A probe for NADH and H<sub>2</sub>O<sub>2</sub> amperometric detection at low applied potential for oxidase and dehydrogenase based biosensor applications, *Biosens. Bioelectron.* 22 (2007) 854–862.
- [10] H.M. Nassef, A. Radi, C.K. O'Sullivan, Electrocatalytic sensing of NADH on a glassy carbon electrode modified with electrografted o-aminophenol film, *Electrochem. Commun.* 8 (2006) 1719–1725.
- [11] L. Zhu, J. Zhai, R. Yang, C. Tian, L. Guo, Electrocatalytic oxidation of NADH with meldola's blue functionalized carbon nanotubes electrodes, *Biosens. Bioelectron.* 22 (2007) 2768–2773.
- [12] B. Prieto-Simon, J. Macanas, M. Munoz, E. Fabregas, Evaluation of different mediator-modified screen-printed electrodes used in a flow system as amperometric sensors for NADH, *Talanta* 71 (2007) 2102–2107.
- [13] R.A. Rincon, K. Artyushkova, M. Mojica, M.N. Germain, S.D. Minter, P. Atanassov, Structure and electrochemical properties of electrocatalysts for NADH oxidation, *Electroanalysis* 22 (2010) 799–806.
- [14] H. Jaegfeldt, T. Kuwana, G. Johansson, Electrochemical stability of catechols with a pyrene side chain strongly adsorbed on graphite electrodes for catalytic oxidation of dihydronicotinamide adenine dinucleotide, *J. Am. Chem. Soc.* 105 (1983) 1805–1814.
- [15] L. Gorton, E. Dominguez, Electrocatalytic oxidation of NAD(P)/H at mediator-modified electrodes, *Rev. Mol. Biotechnol.* 82 (2002) 371–392.
- [16] J. Wang, Carbon-nanotube based electrochemical biosensors: a review, *Electroanalysis* 17 (2005) 7–14.
- [17] L. Wu, X. Zhang, H. Ju, Detection of NADH and ethanol based on catalytic activity of soluble carbon nanofiber with low overpotential, *Anal. Chem.* 79 (2007) 453–458.
- [18] M. Musameh, J. Wang, A. Merkoci, Y. Lin, Low-potential stable NADH detection at carbon-nanotube-modified glassy carbon electrodes, *Electrochem. Commun.* 4 (2002) 743–746.
- [19] J. Wang, M. Musameh, A reagentless amperometric alcohol biosensor based on carbon-nanotube/teflon composite electrodes, *Anal. Lett.* 36 (2003) 2041–2048.
- [20] J. Liu, S. Tian, W. Knoll, Properties of polyaniline/carbon nanotube multilayer films in neutral solution and their application for stable low-potential detection of reduced-nicotinamide adenine dinucleotide, *Langmuir* 21 (2005) 5596–5599.
- [21] P. Du, S. Liu, P. Wu, C. Cai, Single-walled carbon nanotubes functionalized with poly(nile blue A) and their application to dehydrogenase-based biosensors, *Electrochim. Acta* 53 (2007) 1811–1823.
- [22] L. Agui, P. Yanez-Sedeno, J.M. Pingarron, Role of carbon nanotubes in electroanalytical chemistry: a review, *Anal. Chim. Acta* 622 (2008) 11–47.
- [23] B. Shlyahovsky, E. Katz, Y. Xiao, V. Pavlov, I. Willner, Optical and electrochemical detection of NADH and of NAD<sup>+</sup>-dependent biocatalyzed processes by the catalytic deposition of copper on gold nanoparticles, *Small* 1 (2005) 213–216.
- [24] L. Tang, G. Zeng, G. Shen, Y. Zhang, Y. Li, C. Fan, C. Liu, C. Niu, Highly sensitive sensor for detection of NADH based on catalytic growth of Au nanoparticles on glassy carbon electrode, *Anal. Bioanal. Chem.* 393 (2009) 1677–1684.
- [25] A.K. Das, C.R. Raj, Facile growth of flower-like Au nanocrystals and electroanalysis of biomolecules, *J. Electroanal. Chem.* 638 (2010) 89–194.
- [26] M.J. Lobo-Castanon, A.J. Miranda-Ordieres, P. Tunon-Blanco, A bienzyme-poly(o-phenylenediamine)-modified carbon paste electrode for the amperometric detection of L-lactate, *Anal. Chim. Acta* 346 (1997) 165–174.
- [27] A. Ciszewski, G. Milczarek, Electrocatalysis of NADH oxidation with an electropolymerized film of 1,4-bis(3,4-dihydroxyphenyl)-2,3-dimethylbutane, *Anal. Chem.* 72 (2000) 3203–3209.
- [28] F. Valentini, A. Salis, A. Curulli, G. Palleschi, Chemical reversibility and stable low-potential NADH detection with nonconventional conducting polymer nanotubule modified glassy carbon electrodes, *Anal. Chem.* 76 (2004) 3244–3248.
- [29] V.S. Vasantha, S.M. Chen, Synergistic effect of a catechin-immobilized poly(3,4-ethylenedioxythiophene)-modified electrode on electrocatalysis of NADH in the presence of ascorbic acid and uric acid, *Electrochim. Acta* 52 (2006) 665–674.
- [30] L. Agui, P. Farfal, P. Yanez-Sedeno, J.M. Pingarron, Poly-(3-methylthiophene)/carbon nanotubes hybrid composite-modified electrodes, *Electrochim. Acta* 52 (2007) 7946–7952.
- [31] K.M. Manesh, P. Santhosh, A. Gopalan, K.P. Lee, Electrocatalytic oxidation of NADH at gold nanoparticles loaded poly(3,4-ethylenedioxythiophene)-poly(styrene sulfonic acid) film modified electrode and integration of alcohol dehydrogenase for alcohol sensing, *Talanta* 75 (2008) 1307–1314.
- [32] S. Mu, Y. Zhang, J. Zhai, Electrocatalysis of NADH oxidation by nanostructured poly(aniline-co-2-amino-4-hydroxybenzenesulfonic acid) and experimental evidence for the catalytic mechanism, *Electrochem. Commun.* 11 (2009) 1960–1963.
- [33] G. Milczarek, Electrochemical conversion of poly-aniline into a redox polymer in the presence of nordihydroguaiaretic acid, *J. Electroanal. Chem.* 626 (2009) 143–148.
- [34] M.D. Rubianes, M.C. Strumia, Polyethylenimine functionalized with dopamine: characterization and electrocatalytic properties, *Electroanalysis* 22 (2010) 1200–1206.
- [35] W. Vastarella, R. Nicastrì, Enzyme/semiconductor nanoclusters combined systems for novel amperometric biosensors, *Talanta* 66 (2005) 627–633.
- [36] K. Schubert, W. Khalid, Z. Yue, W.J. Parak, F. Lisdat, Quantum-dot-modified electrode in combination with NADH-dependent dehydrogenase reactions for substrate analysis, *Langmuir* 26 (2010) 1395–1400.
- [37] Knauth, Rajh, in: M. Baraton (Ed.), *Synthesis, Functionalization and Surface Treatment of Nanoparticles*, American Scientific Publishers, 2003, pp. 127–171 (Chapters 8 and 9).
- [38] Z. Jiang, C. Lu, H. Wu, Photoregeneration of NADH using carbon-containing TiO<sub>2</sub>, *Ind. Eng. Chem. Res.* 44 (2005) 4165–4170.
- [39] D. Chen, D. Yang, Q. Wang, Z. Jiang, Effects of boron doping on photocatalytic activity and microstructure of titanium dioxide nanoparticles, *Ind. Eng. Chem. Res.* 45 (2006) 4110–4116.
- [40] Y. Dilgin, L. Gorton, G. Nisli, Photoelectrocatalytic oxidation of NADH with electropolymerized toluidine blue O, *Electroanalysis* 19 (2007) 286–293.
- [41] D. Gligor, Y. Dilgin, I.C. Popescu, L. Gorton, Photoelectrocatalytic oxidation of NADH at a graphite electrode modified with a new polymeric phenothiazine, *Electroanalysis* 21 (2009) 360–367.
- [42] G. Wang, J. Xu, H. Chen, Dopamine sensitized nanoporous TiO<sub>2</sub> film on electrodes: photoelectrochemical sensing of NADH under visible irradiation, *Biosens. Bioelectron.* 24 (2009) 2494–2498.
- [43] T. Lijima, S. Hamakawa, M. Tomoi, Preparation of poly(1,4-cyclohexylenedimethylene phthalate)s and their use as modifiers for aromatic diamine-cured epoxy resin, *Polym. Int.* 49 (2000) 871–880.
- [44] P. Manisankar, C. Vedhi, G. Selvanathan, R.M. Somasundaram, Electrochemical and electrochromic behavior of novel poly(aniline-co-4,4'-diaminodiphenyl sulfone), *Chem. Mater.* 17 (2005) 1722–1727.
- [45] P. Manisankar, C. Vedhi, G. Selvanathan, H.G. Prabu, Copolymerization of aniline and 4,4'-diaminodiphenyl sulphone and characterization of formed nano size copolymer, *Electrochim. Acta* 52 (2006) 831–838.
- [46] S. Palaniappan, P. Manisankar, Electropolymerisation and characterisation of nanosize conducting poly[(o-chloroaniline)-co-(4,4'-diaminodiphenylsulfone)] on a polyaniline-modified electrode, *Polym. Int.* 59 (2010) 456–462.
- [47] H. Lee, T. Hur, S. Kim, J. Kim, H. Lee, *Catal. Today* 84 (2003) 173–180.
- [48] R. West, X. Zeng, Controlled electrochemical synthesis of polypyrrole nanoparticle thin film and its redox transition to a highly conductive and stable polypyrrole variant, *Langmuir* 24 (2008) 11076–11081.
- [49] C. Zhao, Z. Jiang, Polymerization and redox behavior of polypyrrole (PPy) films by in situ EQCM and PT techniques, *Appl. Surf. Sci.* 229 (2004) 372–376.
- [50] G.Z. Sauerbrey, Verwendung von Schwingquarzen zur Wagung dünner Schichten und zur Mikrowagung, *Z. Phys.* 155 (1959) 206–222.
- [51] Y. Umasankar, A.P. Periasamy, S.M. Chen, Poly(malachite green) at nafion doped multi-walled carbon nanotube composite film for simple aliphatic alcohols sensor, *Talanta* 80 (2010) 1094–1101.
- [52] P.D. Christy, N.S.N. Jothi, N. Melikechi, P. Sagayaraj, Synthesis, structural and optical properties of well dispersed anatase TiO<sub>2</sub> nanoparticles by non-hydrothermal method, *Cryst. Res. Technol.* 44 (2009) 484–488.
- [53] B. Tan, Y. Wu, Dye-sensitized solar cells based on anatase TiO<sub>2</sub> nanoparticle/nanowire composites, *J. Phys. Chem. B* 110 (2006) 15932–15938.
- [54] E. Katz, I. Willner, Probing biomolecular interactions at conductive and semiconductive surfaces by impedance spectroscopy: routes to impedimetric immunosensors, DNA-sensors, and enzyme biosensors, *Electroanalysis* 15 (2003) 913–947.
- [55] H.O. Finklea, D.A. Snider, J. Fedyk, Characterization of octadecanethiol-coated gold electrodes as microarray electrodes by cyclic voltammetry and ac impedance spectroscopy, *Langmuir* 9 (1993) 3660–3667.
- [56] J. Grodkowski, P. Neta, B.W. Carlson, L. Miller, One-electron transfer reactions of the couple NAD<sup>+</sup>/NADH, *J. Phys. Chem.* 87 (1983) 3135–3138.
- [57] A.V. Umrikhina, A.N. Luganskaya, A.A. Krasnovsky, ESR signals of NADH and NADPH under illumination, *FEBS Lett.* 260 (1990) 294–296.
- [58] C.E. Banks, R.G. Compton, *Analyst* 130 (2005) 1232–1239.
- [59] X. Zhu, Y. Yang, M. Zhang, J. Cheng, *J. Am. Chem. Soc.* 125 (2003) 15298–15299.
- [60] A. Gopalan, D. Ragupathy, H.-T. Kim, K.M. Manesh, K.-P. Lee, *Spectrochim. Acta A* 74 (2009) 678–684.
- [61] E.V. Bakmutova-Albert, D.W. Margerum, J.G. Auer, B.M. Applegate, *Inorg. Chem.* 47 (2008) 2205–2211.
- [62] N. Takahashi, T. Shinno, M. Tackikawa, T. Yuzawa, H.J. Takahashi, *Raman Spectrosc.* 37 (2006) 283–290.
- [63] E. Silverstein, Separation and purification of oxidized and reduced nicotinamide adenine dinucleotides, *Anal. Biochem.* 12 (1965) 199–212.
- [64] S. Vijaya, T. Ramasarma, *J. Inorg. Biochem.* 20 (1984) 247–254.

## Biographies

**Ya-Hui Ho** received her Master degree in Chemical Engineering in 2010 from the Department of Chemical Engineering and Biotechnology, National Taipei University of Technology, Taiwan. Her research interests include development of biosensors based on redox enzymes with conducting polymer and multiwalled carbon nanotubes composites.

**Arun Prakash Periasamy** received his Bachelor Degree in Chemistry in 2000 from Government Arts College, Udumalpet, affiliated to Bharathiar University, Tamil Nadu, India. He received his Master Degree and Master of Philosophy Degree in Chemistry in 2003 and 2005 respectively, from Ramakrishna Mission Vidyalaya College of Arts and Science, affiliated to Bharathiar University, Tamil Nadu, India. He is currently a fulltime Ph.D. student in the research group of Dr.

Shen-Ming Chen at the Department of Chemical Engineering and Biotechnology, National Taipei University of Technology, Taiwan. His research interests include study of the direct electrochemistry of redox enzymes and proteins at multiwalled carbon nanotubes, graphene and nano metal oxide composites for biosensor applications.

**Dr. Shen-Ming Chen** received his Bachelor Degree in Chemistry in 1980 from National Kaohsiung Normal University, Taiwan. He received his Master Degree (1983) and Ph.D. Degree (1991) in Chemistry from National Taiwan University, Taiwan. He is currently a professor at the Department of Chemical Engineering and Biotechnology, National Taipei University of Technology, Taiwan. His current research interests include electroanalytical chemistry, bioelectrochemistry, fabrication of energy conservation and storage devices and nanomaterial synthesis for electrochemical applications. He has published more than 170 research articles in SCI journals.

www.spm.com.cn